THE CLOUDSAT MISSION AND THE A-TRAIN

A New Dimension of Space-Based Observations of Clouds and Precipitation

BY GRAEME L. STEPHENS, DEBORAH G. VANE, RONALD J. BOAIN, GERALD G. MACE, KENNETH SASSEN, ZHIEN WANG, ANTHONY J. ILLINGWORTH, EWAN J. O'CONNOR, WILLIAM B. ROSSOW, STEPHEN L. DURDEN, STEVEN D. MILLER, RICHARD T. AUSTIN, ANGELA BENEDETTI, CRISTIAN MITRESCU, AND THE CLOUDSAT SCIENCE TEAM

When launched in 2004, CloudSat—part of the new A-train constellation—will provide much needed measurements of the vertical structure of clouds from space.

One of the more stunning features of the images of earth from space are the clouds that move around our planet in quasi-organized large-scale systems (e.g., Rossow and Cairns 1995). The character and movement of these coherent cloud features are primarily governed by the large-scale atmospheric circulation and, as such, are an essential manifestation of weather systems. Motions of synoptic-scale cloud masses, in turn, trace the circulation patterns of the atmosphere. By tracking movements of individual cloud elements we can also determine the wind fields (e.g., Menzel 2001).

These large cloud systems are not mere passive tracers of wide-scale movement of air. They exert an enormous influence on our weather and climate. Clouds are a fundamental stage of the cycle of water in the atmosphere, condensing water vapor and forming precipitation. Clouds also dominate the energy budget of the planet. They tend to cool the earth by reflecting sunlight back to space while simultaneously warming the earth by absorbing and reemitting thermal radiation emitted by the surface and lower atmosphere (for more on this complex process see Wielicki et al. 1995). By modulating the distribution of heating within the atmosphere and at the surface, clouds fundamentally influence the circulations of the atmosphere and oceans. The importance of clouds to the resultant redistribution of heating is underscored in the study of Glecker et al. (1995). They showed how poorly resolved clouds, through their effects on the surface radiation budget, produce an unacceptable discrepancy

AFFILIATIONS: STEPHENS, AUSTIN, BENEDETTI, MITRESCU, AND THE CLOUDSAT SCIENCE TEAM—Department of Atmospheric Science, Colorado State University, Fort Collins, Colorado; VANE, BOAIN, AND DURDEN—Jet Propulsion Laboratory, California Institute of Technology, Pasadena, California; MACE, SASSEN, AND WANG—Department of Meteorology, University of Utah, Salt Lake City, Utah; ILLINGWORTH AND O'CONNOR—Department of Meteorology, University of Reading, Reading, Berkshire, United Kingdom; ROSSOW—NASA Goddard Institute for Space Studies, Columbia, New York; MILLER—Naval Research Laboratory, Monterey, California
CORRESPONDING AUTHOR: Dr. Graeme L. Stephens, Department of Atmospheric Science, Colorado State University, Fort Collins, CO 80523-1371
E-mail: stephens@atmos.colostate.edu
DOI: 10.1175/BAMS-83-12-1771

In final form 8 August 2002

in the implied oceanic transport of heat poleward as simulated by a large number of climate models.

Despite the fundamental role of clouds in climate, there is much that we do not know. Much of our current global perspective derives from spectral radiances measured by sensors on satellites. This global view, provided, for example, by the ISCCP (see appendix A for acronym expansions; Rossow and Schiffer 1999), quantifies optical properties integrated through the atmospheric column. Furthermore, Earth Radiation Budget measurements (e.g., Harrison et al. 1993; Wielicki et al. 1995; Kandel et al. 1998) also monitor incoming and outgoing radiation at the top of the atmosphere and the effects of clouds on these outgoing fluxes. Neither type of data, however, indicates how the radiant energy is vertically distributed within the atmosphere, knowledge that is fundamental to the study of climate.

Clouds also influence climate variability and change by affecting the efficiency at which the hydrological cycle operates. TRMM (Simpson et al. 1996) has quantified how much precipitation falls in the tropical atmosphere. We cannot estimate within a factor of 2 the mass of water and ice in these clouds (e.g., Stephens et al. 1998) let alone how much of this water and ice is converted to precipitation. We also cannot say with any certainty what fraction of global cloudiness produce precipitation that falls to the ground.

A new satellite-based cloud experiment, hereafter the CloudSat mission, aims to provide observations necessary to advance our understanding of these issues. The CloudSat mission was selected under NASA ESSP Program (see online at http://essp.gsfc.nasa.gov) with a scheduled launch for 2004. CloudSat will fly the first spaceborne millimeter wavelength radar. The unique feature of this radar lies in its ability to observe jointly most of the cloud condensate and precipitation within its nadir field of view and its ability to provide profiles of these properties with a vertical resolution of 500 m. The CloudSat satellite flies as part of a constellation of satellites that includes the EOS *Aqua* and *Aura* at each end of the constellation, CloudSat, a second ESSP mission that flies an aerosol lidar (CALIPSO), and another small satellite, PARASOL, carrying the POLDER polarimeter (Deschamps et al. 1994) inserted in the formation between the larger EOS spacecraft (Fig. 1). This constellation is referred to as the A-Train. Table 1 summarizes the sensor complement of the A-Train and the types of cloud and aerosol products available from each sensor. Combining the observations of the different sensors of the A-Train with the millimeter radar observations is a key aspect of the observing philosophy of the CloudSat mission.

THE NATURE OF THE CLOUDSAT SCIENCE. Predictions of global warming using climate models forced with increased CO_2 are uncertain (Fig. 2a) and the range of uncertainty has not changed much from estimates given more than two decades ago. One of the main reasons for this continued uncertainty is the inadequate way clouds and their radiative properties are represented (e.g., Webster and Stephens 1983; Cess et al. 1989; Senior and Mitchell 1993; IPCC, see online at www.ipcc.ch). Even small changes in the abundance and/or distribution of clouds profoundly alter the climate response to changes in greenhouse gases, anthropogenic aerosols, or other factors (Fig. 2b). Studies also indicate how coupled ocean–atmosphere models are even more acutely sensitive to cloud parameters (e.g., Ma et al. 1994).

One key to unraveling the complexity of cloud feedback lies in clarifying the association between atmospheric circulation regimes and cloudiness. This requires a more quantitative understanding of the relationships between clouds, total diabatic heating, and circulation (schematically portrayed in Fig. 3). However, since the relationships depicted in Fig. 3 are primarily a manifestation of the *weather* systems that form the vast cloud masses, a fruitful strategy to study and understand them should also embrace NWP and related activities. Providing *relevant* observations that link this large-scale view of the circulation to cloud

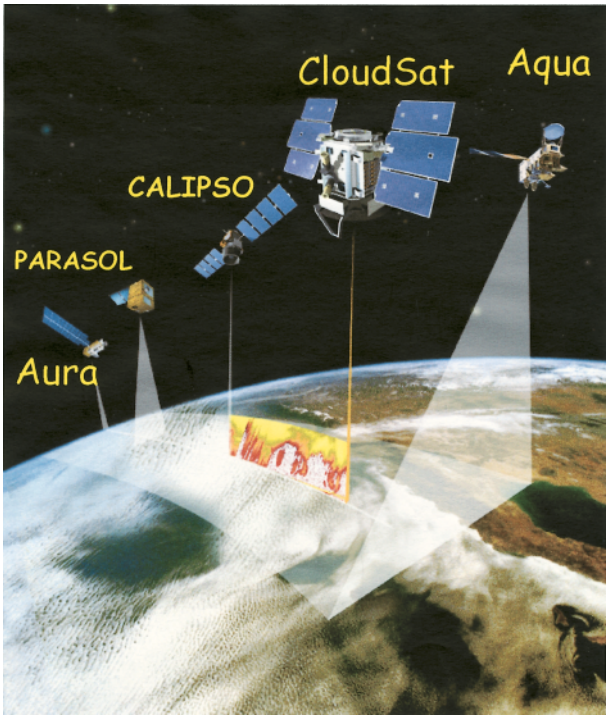

Fig. 1. The concept of the A-Train constellation and its members.

Table 1. Sensor complement and related products of the A-Train.

Spacecraft	Payload	Characteristics	Cloud and aerosol products
Aqua Lead constellation spacecraft	MODIS	36-channel visible radiometer, 2300-km-wide swath, variable resolution from 0.25 to 1 km.	Land, ocean, and atmospheric products. The latter include cloud and aerosol optical depths and particle size information, as well as cloud emissivity and cloud-top height.
	AIRS/ AMSU-A/ HSB	Combination of IR and microwave sounders. Swath of ±50°, resolution of IR sounder ~10 km.	Temperature and moisture profiles in clear atmosphere. Some cloud properties.
	AMSR-E	6-channel microwave radiometer. 1445-km swath, asymmetric FOV with variable resolution from ~6 × 4 km (89 GHz) to 43 × 75 km (6 GHz).	LWP, column water vapor, liquid precipitation, principally confined to ocean regions.
	CERES	Broadband and spectral radiances converted to fluxes, resolutions at nadir – 20 km.	TOA radiation budget. Primary product is time mean fluxes but instantaneous fluxes are also produced.
CloudSat Lags *Aqua* by a variable amount but less than 120 s	94-GHz radar (CPR)	500-m vertical range gates from surface to 30 km. High sensitivity, FOV approximately 1.4 km.	Cloud profile information, liquid and ice water content profiles, precipitation. The information is obtained by combining the radar measurements with *Aqua* measurements including MODIS and AMSR-E as well as with the CALIPSO lidar.
CALIPSO Separation is maintained by CloudSat. Lags CloudSat by 15 ± 2.5 s	Lidar (CALIOP)	532- and 1064-nm channels with depolarization. FOV of approximately 300- and 70-m resolution.	Cloud profile information primarily of upper-tropospheric clouds. Optical depth of thin cirrus. Aerosol profiles with attached optical depth estimates. Aerosol information requires averaging over 10s of kms especially in daylight.
	IIR	3-channel IR radiometer with a FOV of 1 km, swath 64 km.	Cirrus cloud optical properties.
PARASOL Lags CALIPSO by ~2 min	POLDER	9-channel polarimeter with channels in the visible and near-infrared. Resolution of 5 m, swath of 400 km.	Cloud and fine mode aerosol optical depths and particle sizes.
Aura Lags Aqua by about 15 min	HIRDLS	IR limb sounder.	Trace gases and stratospheric aerosol.
	MLS	Microwave limb sounder.	Trace gases, ice content of thin upper-tropospheric cloud.
	TES	IR imaging spectrometer, 0.5 × 5 km resolution, narrow swath and variable pointing.	Trace gases, could also provide high spectral resolution data on clouds.
	OMI	UV grating spectrometer, 13 × 24 km resolution.	Ozone and aerosol index.

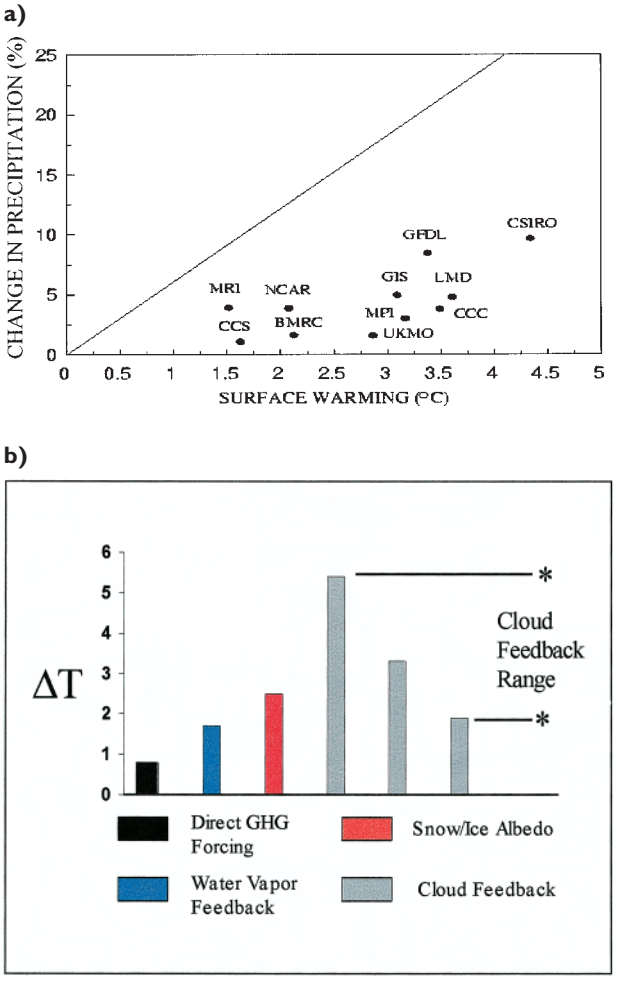

FIG. 2. (a) The responses of various coupled ocean–atmosphere GCMs to an imposed doubling of CO_2. The different models can be identified according to the indicated organization. (b) The response of a single climate model to an imposed doubling of CO_2 as different feedbacks are systematically added in the model (starting from left to right and adapted from Senior and Mitchell 1993). Different treatments of cloud processes in the model produce a large spread in predicted surface temperature due to CO_2 doubling.

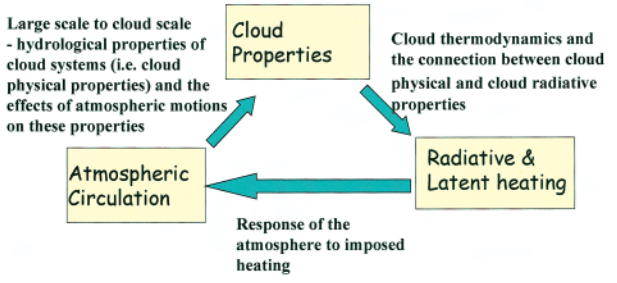

FIG. 3. A schematic depiction of the main elements of the cloud-feedback problem. The links between the boxes indicate processes that are the key to the way these feedbacks are established.

heating is a key objective of CloudSat. Forging partnerships with major NWP centers, in addition to major climate modeling groups, is thus an essential ingredient of the CloudSat strategy.

The importance of cloud profile information. One of the main reasons model predictions of climate warming vary from model to model is the different ways models specify vertical cloud distributions. The vertical distribution and overlap of cloud layers directly determine both the magnitude and vertical profile of radiative heating (Slingo and Slingo 1988; Stephens 2001; Fig. 4a). For example, high cloud layers heat the tropical atmosphere by more than 80 W m^{-2} (relative to clear skies; Stephens 1999). This heating exerts a dominant influence on the large-scale, "Hadley" circulation of the atmosphere (Randall et al. 1989) as well as on deep convective cloud systems (Grabowski et al. 2000). Other processes are also affected by the vertical distribution of heating (e.g., Liang and Wang 1997), notably through the connections between convection and precipitation (e.g., Fowler and Randall 1994; Parsons et al. 2000).

The assumed vertical distribution of a cloud also influences precipitation predicted by models. For example, assumptions about the cloud vertical structure directly influence the seeder–feeder precipitation mechanism in large-scale models (Jakob and Klein 1999). Figure 4b illustrates the substantial sensitivity of the forecast precipitation to the assumption of cloud overlap.

These two examples illustrate the importance of cloud profile information—even if limited to cloud occurrence. Direct measurements of the vertical structure of clouds have, until now, been limited to a few ground-based radar sites. More indirect efforts to obtain a global-scale view of vertical cloud structure rely on water vapor variations observed in global radiosonde data. Poore et al. (1995) and Wang et al. (2000) indicate that overlapping cloud layers occur about 40% of the time but vary from less than 10% over deserts and mountains to over 80% in tropical convective regions. Although these global statistics are broadly consistent with statistics accumulated from surface cloud radar sites (Mace et al. 1999), they require extensive verification with the more direct measurements of CloudSat.

Cloud water content and precipitation. The water content of cloudy air is a parameter fundamental to predicting cloud evolution and other key properties of clouds. For example, various cloud particle growth mechanisms occur at a rate proportional to the wa-

ter content, including the growth of precipitation-sized drops (e.g., Rogers 1979). Furthermore, the radiative properties of clouds are directly related to water contents and the integrals of these water contents along the vertical path (e.g., Stephens 1978).

Models represent clouds as fields of liquid and frozen water with equations that parameterize essential microphysical and turbulent processes (e.g., Sundquist 1978; Fowler et al. 1996; Tiedtke 1993; and others). The parameterizations contain significant uncertainties that, for the most part, cannot be tested on the global scale. According to Fig. 5, the liquid water path varies substantially among models. Although our ability to provide similar information from observations is crude (Stephens et al. 1998), these observations nevertheless possess smaller uncertainties than the model-to-model differences of Fig. 5a. Variations in the TOA radiative fluxes (not shown) and precipitation (Fig. 5b) among the same models are smaller reflecting the heavy tuning of the model to available observations of these quantities. The variability of the cloud properties, compared to radiative properties and precipitation, underscores serious problems in parameterizing the processes that connect radiation, clouds, and precipitation and thus the critical processes portrayed in Fig. 3.

CLOUDSAT SCIENCE OBJECTIVES. CloudSat seeks to help solve these problems and spur improvements in both weather forecasting and climate prediction. It aims to evaluate quantitatively the representation of clouds and cloud processes in global atmospheric circulation models, and the relationship between the vertical profiles of cloud liquid water and ice content and cloud radiative properties, including the radiative heating by clouds. In so doing, CloudSat seeks to provide the first direct global survey of the vertical structure of cloud systems. It will also measure the profiles of cloud liquid water and ice water content and match these profiles of the bulk cloud microphysical properties to cloud optical properties. Optical properties contrasted against cloud liquid water and ice contents are a critical test of key parameterizations that enable calculation of flux profiles and radiative heating rates throughout the atmospheric column. To date, this type of evaluation can only be carried out using data collected in field programs and from surface measurements limited to a few locations worldwide.

These primary objectives are also augmented by other science objectives. CloudSat data provides a rich source of information for evaluating cloud properties derived from other satellite data including those produced from *Aqua* (see also Table 1) as well as cloud information derived from operational sensors. CloudSat information will also improve when data from other sensors are combined with the radar. Connecting CloudSat observations to the cloud properties derived from geostationary satellites also serves a number of important purposes. The geostationary information can be used to evaluate and enhance the cloud sample of CloudSat as well as to project the observations of the CloudSat era onto longer time series of cloud information provided by ISCCP. CloudSat and the A-Train also offer an unprec-

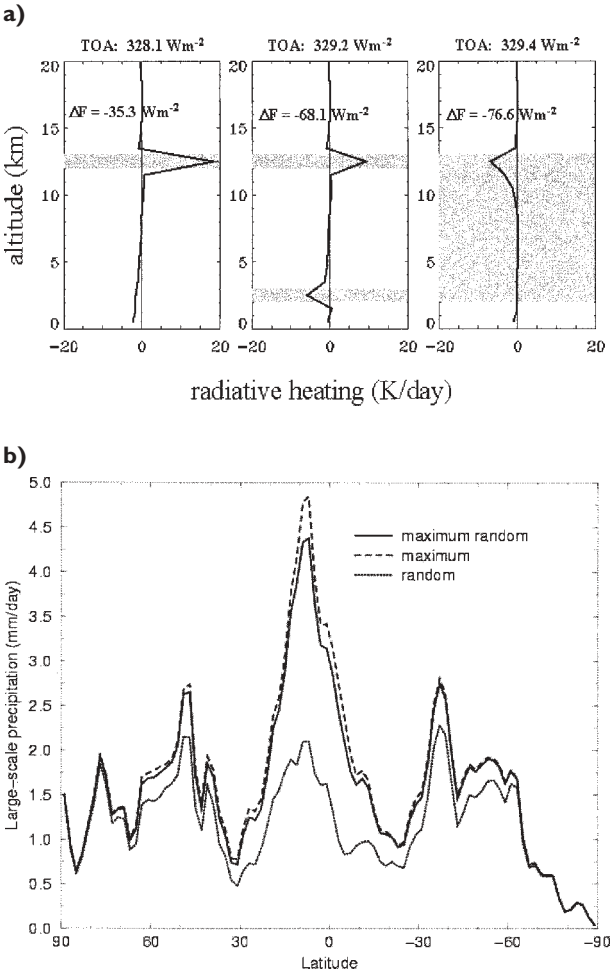

FIG. 4. (a) Vertical profiles of cloud radiative heating rate (K day^{-1}) differ due to the different location and thickness of cloud layers (shaded, and adapted from Slingo and Slingo 1988). The net column flux divergence difference between completely overcast and clear sky (ΔF) is (left) +45 W m^{-2}, (middle) +12 W m^{-2}, and (right) +3 W m^{-2}. (b) Zonal mean large-scale precipitation rate for the first time step of a T63L31 integration with the subgrid precipitation model using maximum-random (solid), maximum (dashed), and random (dotted) cloud overlap.

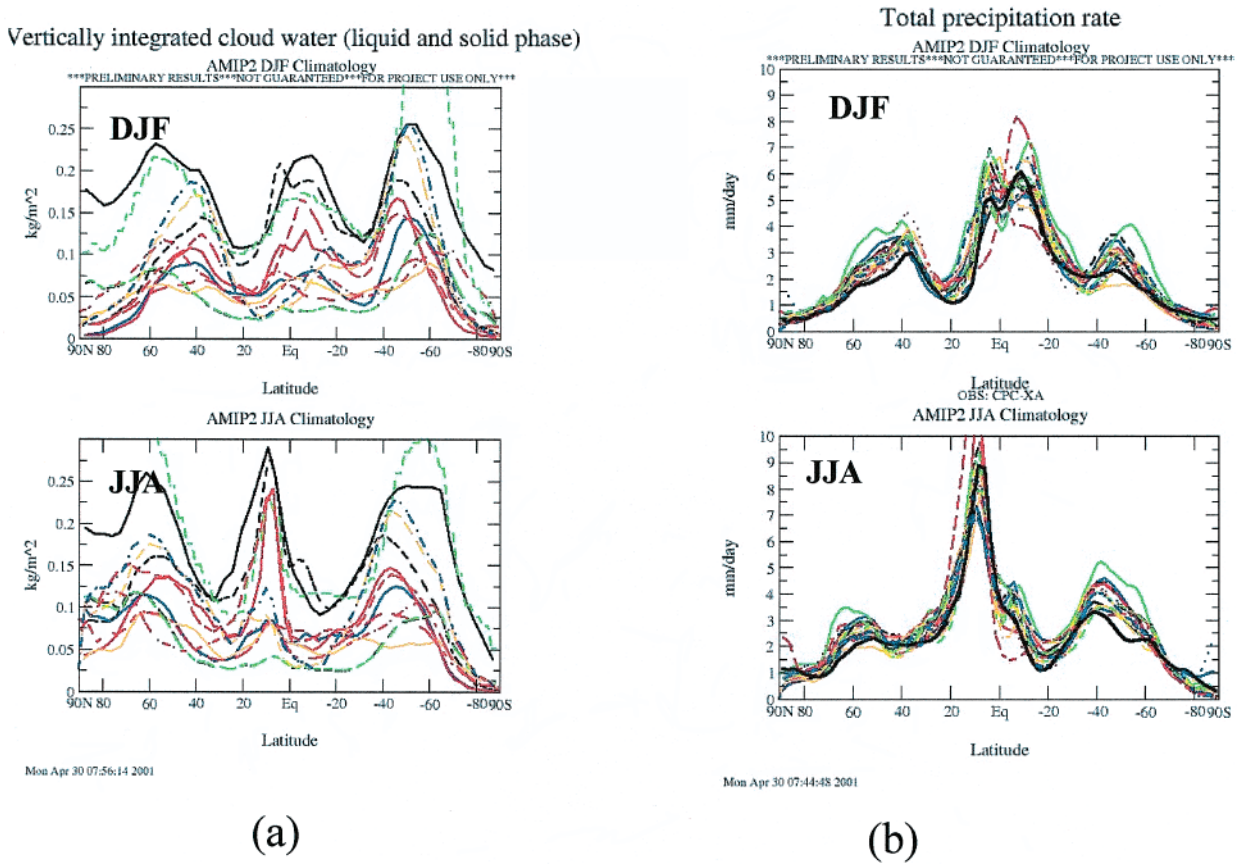

FIG. 5. (a) Comparison of the zonally averaged liquid-plus-solid water paths derived from different GCM simulations submitted to AMIP II. The zonal profile of each model is represented by a colored line. (b) Comparison of the zonally averaged precipitation derived from the same suite of models of (a). In this case a profile derived from "observations" is included.

edented resource for understanding the potential of aerosol for changing cloud properties and thus the radiative budget of clouds. The aerosol context provided by other constellation measurements includes MODIS on *Aqua,* the lidar on CALIPSO, the polarimeter on PARASOL, and aerosol chemistry from *Aura* measurements. This information can be combined with the cloud water, ice, and precipitation information of CloudSat and AMSR-E to a lesser degree, cloud optical property information of MODIS and PARASOL, and the CERES radiative fluxes to explore aerosol–chemistry–cloud interactions.

THE MISSION. Although the original CloudSat concept included the combination of lidar and radar and even precipitation measurements (GEWEX 1994) this proved too costly. Also due to cost constraints imposed by ESSP, contributions to specific portions of the mission were required.

Partnerships. The partnerships of CloudSat are reflected in the schematic mission overview of Fig. 6. The JPL of the California Institute of Technology is developing the payload and managing the project. The CSA is contributing key components and subsystems of the radar. Ball Aerospace provides the spacecraft bus, which is the fifth in the RS2000 line of spacecraft used both for QuikScat and ICESat. Ball Aerospace is also responsible for spacecraft integration and testing. The U.S. Air Force Space Test Program is providing ground operations and is managing communications with the spacecraft. The data will be downlinked several times per day through S-band links as part of the U.S. Air Force SGLS network of receiving stations. Validation activities take advantage of ground-based observational sites such as the DOE CART sites as part of the ARM program (Stokes and Schwartz 1994), NASA and ARM airborne science campaigns, and various national and international university and government research facilities reflected in the science team membership.

The mission was conceived and proposed by the lead author located at Colorado State University. CIRA, also located at CSU, will process all CloudSat

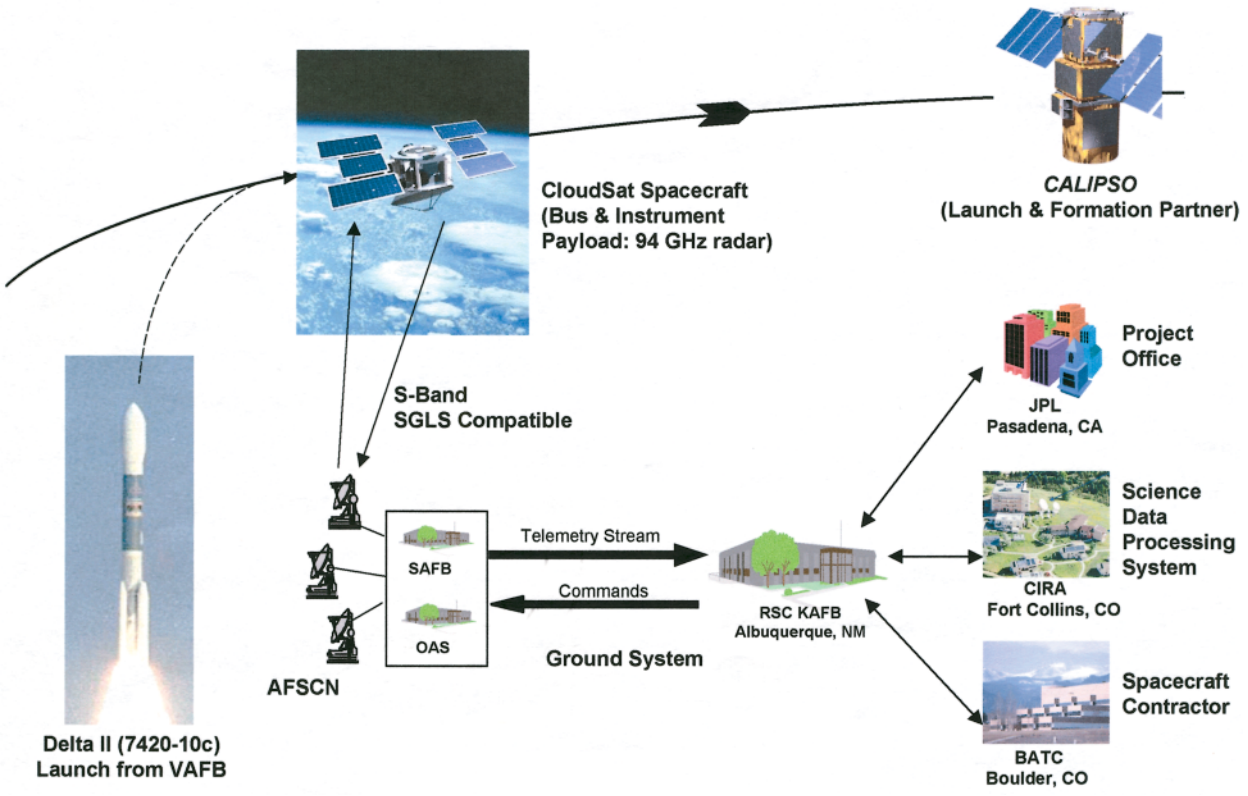

FIG. 6. The Mission overview: The launch is from VAFB and data are transmitted via the spacecraft S-band downlink to the AFSCN and then to the RSC and KAFB in Albuquerque, NM. The data are then distributed to CIRA for science processing, with mission and state-of-health information being sent to BATC in Boulder, CO, and to NASA's JPL in Pasadena, CA.

level-0 data and higher-level data products (i.e., levels 1–3). The DPC system design is based on the current CIRA satellite earth station model, which has been operational since 1994.

All CloudSat standard data product generation software will be hosted on a software application referred to as CORE, which is a derivative of the DPEAS (Jones and VonderHaar 2001). The DPEAS currently processes 17 TB of data from various satellites per year. CORE is centered on the HDF-EOS format and is based on a parallel computing environment that has a number of distinct and desirable advantages, including an ability to build redundancy of processors, to accommodate failures, and to expand the cluster in response to growth in data processing needs achieved with easy access to inexpensive scalable computing resources. Under the current plan, data will be made available to the CloudSat Science Team followed by a release to the scientific community via the Langley DAAC within 6 weeks after the science team has assessed the data and its validation.

Formation flying. In formation flying, two or more spacecraft move in matched orbits. One spacecraft is burdened to make routine adjustments to maintain a predetermined geometry with respect to the other. CloudSat is the burdened spacecraft in the A-Train maintaining a formation with *Aqua* and CALIPSO to overlay radar footprints with the lidar footprints of CALIPSO at least 50% of the time as well as to make the radar footprints fall in the central few kilometers of the *Aqua* MODIS swath. Because the imaging swath of MODIS is so much broader than the individual footprint of the CALIPSO lidar, CloudSat will control its formation in relation to CALIPSO more precisely than with *Aqua.*

The general formation-flying concept that forms a portion of the A-Train is illustrated in Fig. 7. Both CloudSat and CALIPSO follow *Aqua,* which is in an orbit synchronized to the WRS-2 grid of ground tracks. To fly this grid, *Aqua* uses a sun-synchronous 705-km-altitude orbit with a 13:30 local mean time for crossing the equator. *Aqua's* orbit repeats its ground track every 16 days although not precisely due to atmospheric drag and other lesser effects. As a consequence, *Aqua* performs maneuvers whenever its subsatellite ground track deviates more than 20 km from the WRS-2 reference. This cross-track motion

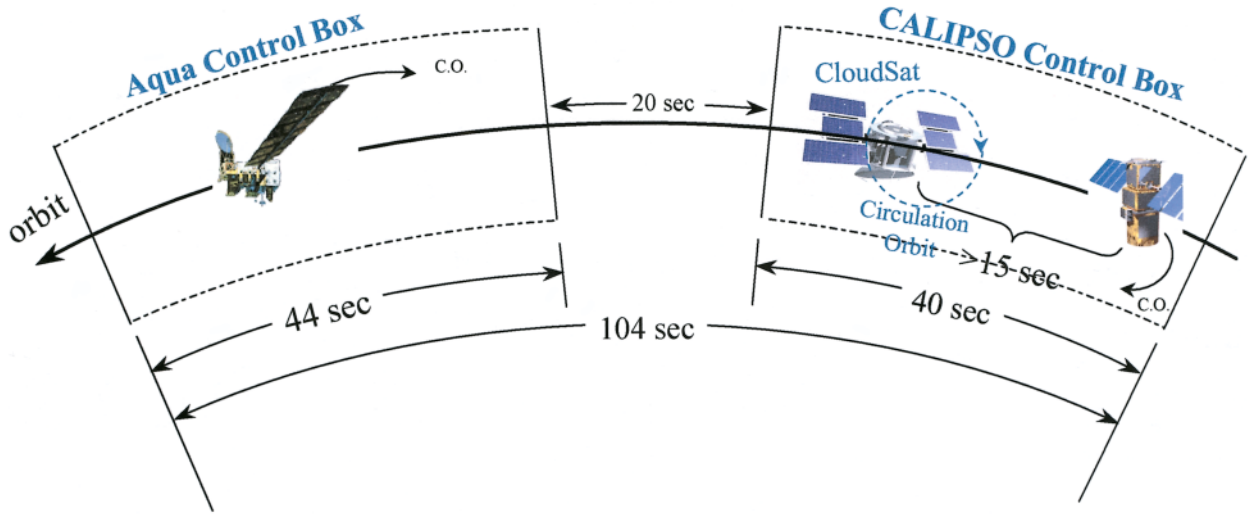

FIG. 7. A schematic of the orbit control boxes of three A-Train satellites indicating the relations between each other. In this depiction, CloudSat maintains a tight formation with respect to CALIPSO.

constraint also defines the deviation of the along-track motion relative to a central position fixed exactly on the WRS-2 grid to 44 s back and forth from a central reference position. This ±44 s deviation in the along-track direction defines *Aqua's* "control box" relative to the WRS-2 grid (Fig. 7). In practice, *Aqua's* cross-track deviations are to be controlled relative to the WRS-2 to be less than ±10 km, well within the ±20 km requirement, reducing the along-track deviation to just ±22 s, thus creating a smaller control box.

CloudSat is to trail *Aqua* by less than 120 s and will maneuver to just 15 s ahead of CALIPSO. CloudSat will then maintain a tight formation with CALIPSO by controlling its cross-track motion to within ±1 km of the CALIPSO ground track. This is achieved by placing CloudSat in a small circulation orbit relative to CALIPSO contained within CALIPSO's control box. This circulation orbit would swing roughly 2.5 s forward and backward of a mean position always 15 s in front of CALIPSO (Fig. 7). Maneuvers to maintain this circulation orbit will be carried out approximately weekly.

Orbit and mission duration. The temporal sampling and global coverage characteristics of CloudSat are dictated by the *Aqua* orbit. The sensitivity of the radar is not as high as it would be in a preferred lower, TRMM-like orbit between 350 and 400 km, but the desire to maximize the radar sensitivity had to be weighed against the value of maximizing synergy with the A-Train.

The CloudSat mission is designed for a 2-yr lifetime to observe more than one seasonal cycle. There is no anticipated technical reason, however, why the mission could not last longer as the radar is expected to operate beyond 3 yr with an approximate 99% probability.

THE CLOUDSAT RADAR. Use of millimeter-wave radar systems over the past decade has flourished leading to a broader understanding of the radar reflection properties of various types of clouds than was available at the time of the early formulation of CloudSat. Cloud radars now operate routinely or quasiroutinely at a number of surface sites worldwide (e.g., Moran et al. 1998). These millimeter-wavelength radars operate at wavelengths of approximately 3 or 8 mm (or frequencies of 94 or 35 GHz, respectively) and are currently deployed on various research aircraft. Measurements collected over a number of years from these research radars provide a rich heritage for CloudSat.

Radar properties. Because clouds are weak scatterers of microwave radiation, the overriding requirement on the radar is to achieve the maximum possible sensitivity and hence maximize cloud detection. Sensitivity is primarily determined by radar-received power and noise level and optimizing this sensitivity involves a careful tradeoff among competing and conflicting factors, including the cloud backscattering properties, the vertical resolution, atmospheric attenuation, available power delivered to the system, the orbit altitude, and radar technology. The received power can be increased by increasing the antenna size and increasing transmitter output power. The antenna diameter of 1.85 m is limited by launch constraints. The transmitter power is also limited by both

the transmitter technology and the power supply capability of the spacecraft.

The amount of power received is also strongly influenced by the cloud reflectivity and atmospheric attenuation. Cloud reflectivity increases with increasing radar frequency but atmospheric attenuation becomes prohibitive at higher frequencies. From these considerations, the operating frequency of 94 GHz is an optimum compromise and provides an increase of 33 dB over the 14-GHz TRMM radar. An international frequency allocation of 94 GHz was subsequently established for spaceborne radar use.

Sensitivity is also related to the pulse length. The radar uses 3.3-μs pulses providing cloud and precipitation information with a 500-m vertical range resolution between the surface and 30 km. The radar measurements along track are averaged in 0.32-s time intervals, producing an oblong effective FOV of approximately 1.4 × 3.5 km. To enhance the capabilities of the system, the radar measurements are also sampled at 250 m in range and 0.16 s along the nadir track.

The power measured by the receiver subsystem of the radar system is converted into a quantity referred to as radar reflectivity Z (e.g., Battan 1973). The performance requirements of the radar are also expressed in terms of Z and one factor that is particularly important is the MDS expressed in terms of reflectivity. The MDS establishes the detection threshold of the instrument and the requirements on the MDS are dictated by the science objectives and related science requirements (appendix A). Based on our current understanding of cloud reflection, the requirement placed on the sensitivity of CPR is –26 dBZ at the end of the mission, a 70-dB dynamic range, and a calibration accuracy of 2 dBZ before launch (with a goal of 1.5 dBZ). The MDS of the CloudSat radar is expected to be between –28 and 29 dBZ early in the mission. By comparison, the TRMM PR has a sensitivity of approximately +20 dBZ. With this sensitivity, the radar detects the majority of clouds that significantly affect the radiation budget and critical elements of the water budget of the atmosphere. Assessment of the impact of those clouds missed by the radar, and the extent these missed clouds are detected by other sensors of the A-Train, is ongoing.

Three of the more noteworthy components of the radar hardware are highlighted in Fig. 8. The antenna subsystem consists of the collimating antenna and the QOTL. The antenna, constructed of composite graphite material, meets the challenge of low surface roughness (less than an rms of 5 μm over the entire surface) and delivers a highly directional beam of half-width less than 0.12°. The antenna also has far-side lobe levels 50 dB below that of the main lobe as required to remove aliasing of these side lobes into the profiles of the following pulse. The QOTL minimizes loss through the system. This will be the first time QOTL technology has flown in space at the wavelength of the radar. Another important challenge in the radar design is the HPA subsystem. The HPA has complete redundancy and consists of two EIKs and two high voltage power supplies. One key development was the redesign of the commercial EIK unit to one qualified to operate in space (Fig. 8).

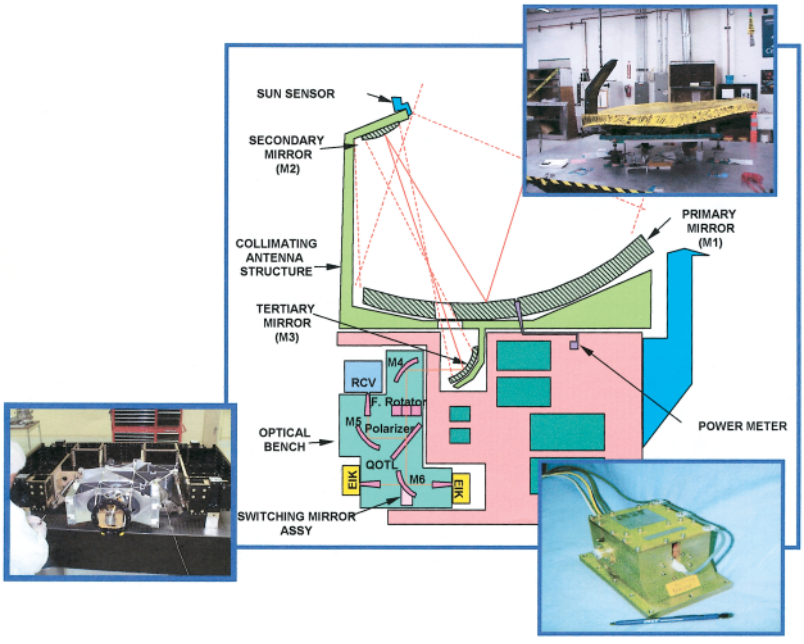

FIG. 8. The radar is composed of the following subsystems: the RFES, the HPA, the antenna subsystem, and the digital subsystem. Shown is a schematic of the antenna and HPA subsystems. The inset figures are actual photographs of flight hardware. The antenna subsystem consists of (top inset) the antenna, and quasi-optical transmission line built on an optical bench (left inset). (lower right inset) EIK, a key component of the HPA, which is required to amplify the transmitted pulse to 1.7 kW. The approximate 2-kW output of the flight model EIK exceeds this requirement.

TABLE 2a: Calculated two-way attenuation (in dB) of a TRMM-like PR radar (14 GHz) and a CloudSat-like radar (94 GHz) derived for a path from the TOA to three representative levels within the atmosphere.

McClatchey profile	14 GHz			94 GHz		
	10 km	5 km	0.5 km	10 km	5 km	0.5 km
Tropical	0.015	0.047	0.293	0.121	0.550	5.454
Midlatitude summer	0.014	0.043	0.231	0.114	0.476	4.084
Midlatitude winter	0.012	0.038	0.137	0.099	0.352	1.820
Subarctic winter	0.011	0.037	0.118	0.091	0.321	1.312

TABLE 2b. Characteristic attenuation of liquid water clouds, ice crystals, and precipitation in terms of the two-way attenuation in a cloud. These can be derived from the given values multiplied by a given water or ice content of the cloud and the two-way geometric pathlength through clouds. Two-way attenuation in precipitation is derived via $\sigma_p^D = k_p R^\gamma$ (dB km^{-1}) multiplied by the two-way geometric pathlength through precipitation. Values of σ_p^D are given for specified rain rates.

Liquid	3 GHz (10 cm)			14 GHz (2.1 cm)			94 GHz (3.2 mm)		
	–8°C	10°C	20°C	–8°C	10°C	20°C	–8°C	10°C	20°C
n	8.94	9.02	8.88	5.39	6.89	7.44	2.53	3.04	3.34
k	1.8	0.9	0.063	3.03	2.78	2.41	1.23	1.75	2.04
Im (–K)	0.013	0.0069	0.0051	0.063	0.035	0.027	0.217	0.177	0.153
k_c^*	0.011	0.0056	0.0042	0.239	0.135	0.102	5.72	4.68	4.05
Ice	**3 GHz (10 cm) –20°C**			**14 GHz (2.1 cm) –20°C**			**94 GHz (3.2 mm) –20°C**		
n	1.78			1.78			1.78		
k	0.0002			0.0007			0.003		
Im(–K)	9.0E-5			0.0003			0.001		
k_c*	7.0E-5			0.0011			0.029		
Rain	**3 GHz (10 cm)**			**14 GHz (2.1 cm)**			**94 GHz (3.2 mm)**		
k_p	0.000004			0.014			0.744		
gamma	1			1.21			0.734		
0.1 mm h^{-1}	4X10^{-7} dB km^{-1}			9X10^{-4} dB km^{-1}			0.137 dB km^{-1}		
1 mm hr^{-1}	4X10^{-6} dB km^{-1}			1.4X10^{-2} dB km^{-1}			0.744 dB km^{-1}		
10 mm h^{-1}	4X10^{-5} dB km^{-1}			0.277 dB km^{-1}			4.033 dB km^{-1}		

* ln (dB km^{-1})/(g m^{-3}).

Attenuation at 94 GHz. At 94 GHz, the two-way attenuation of the radar pulse as it propagates through the atmosphere results from absorption by gases (chiefly water vapor), liquid water droplets, and precipitation-sized particles. Tables 2a and 2b provide some idea of the attenuation expected under typical atmospheric conditions and contrast the attenuation at 94 against that of 14 GHz. The total column two-way attenuation by water vapor can be adequately corrected using profile information derived from operational analyses whereas attenuation by cloud droplets and precipitation (Table 2b) must be included in the design of relevant retrieval algorithms.

Reflectivity of selected cloud types at millimeter wavelengths. Data collected from cloud radar over many years reveal how the reflectivity of clouds varies over several orders of magnitude. This range of reflectivities is exemplified in the time–height radar reflectivity cross section in Fig. 9 obtained from an aircraft millimeter-wave radar flown over a convective cloud complex. The figure illustrates the cloud radar representation of convective precipitation, stratiform precipitation mixed with liquid cloud, and overlying layers of ice clouds. The reflectivity factor ranges from below −30 dBZ around the edges of the upper ice layers to approximately 20 dBZ in heavier precipitation.

Profile data like those in Fig. 9, when accumulated from a large number of flights or from many hours of surface measurements, provide a database for establishing the general reflectivity characteristics of different cloud types. One type of cloud that challenges the sensitivity of the radar is the shallow boundary layer cloud. The accumulation of many hours of aircraft and surface radar data from such clouds are shown in Figs. 10a and 10b. This figure suggests that for a sensitivity of −28 dBZ only about 70% of the low-level water clouds over the ocean and perhaps only 40% or less of these clouds over land are detected. The results of this figure underscore the need for the additional information available from the other sensors of the A-Train.

Similar kinds of composite analyses applied to cirrus cloud radar data highlight the different nature of the radar reflection by these types of clouds. Based on the analyses presented in Fig. 11, the limit of cirrus detection by a CloudSat-like radar generally lies in the

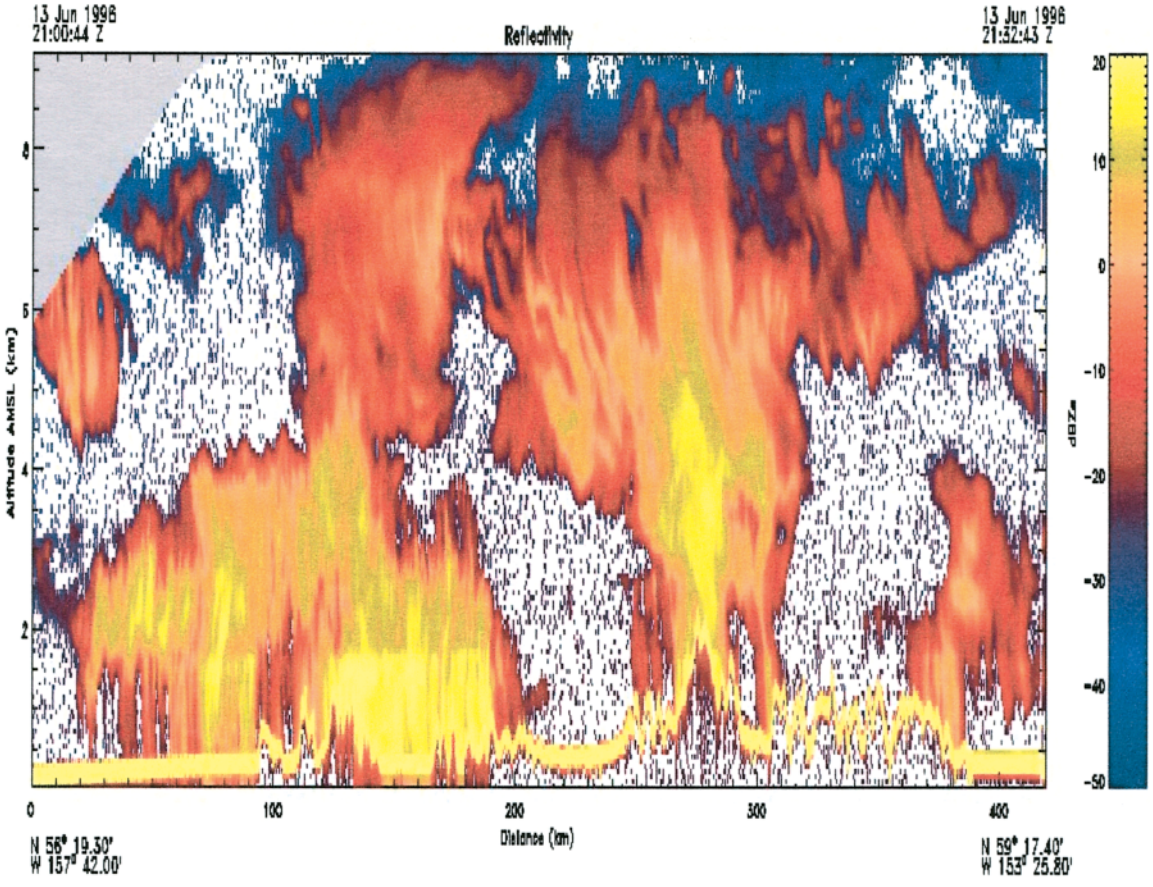

Fig. 9. Time–height cross section of radar reflectivity as measured by a downward-looking 94-GHz radar on NASA's DC-8 research aircraft.

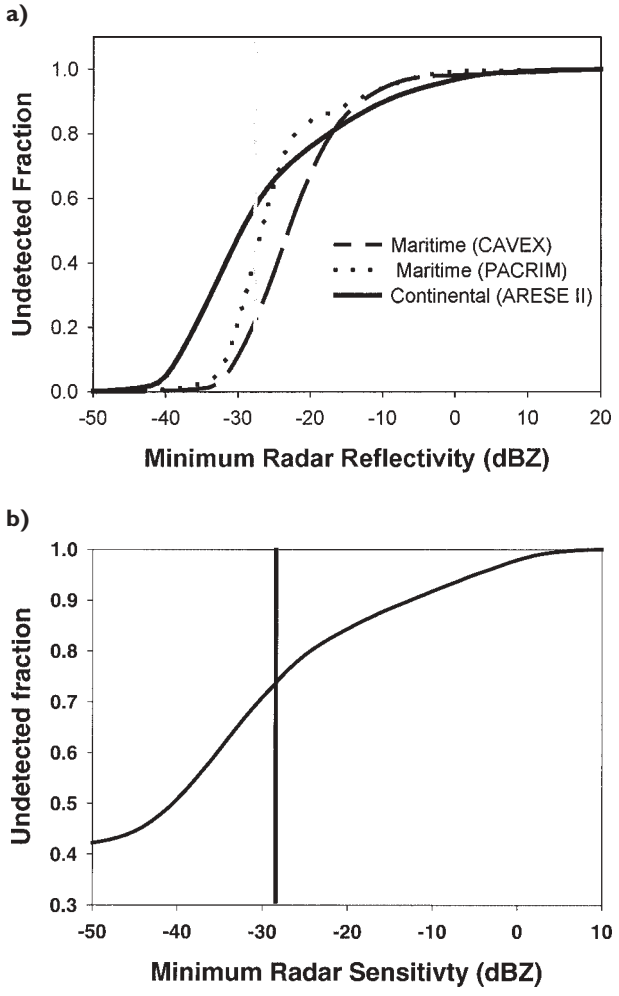

Fig. 10. (a) Examples of reflectivity CDFs constructed from approximately 30 000 reflectivity profiles of marine stratus and stratocumulus observed off the coast of California and over the southern Pacific Ocean in the vicinity of New Zealand. Shown for comparison is a similar reflectivity CDFs derived from more than 17 000 profiles of continental layered clouds observed by the MMCR operated over the DOE ARM CART site. (b) Same as (a) but for low-level water clouds simultaneously detected by both a ground-based lidar and radar. The lidar detection is presented as a function of radar reflectivity. The data are a composite of 6600 h of coincident radar/lidar data over a 15-month period in the United Kingdom.

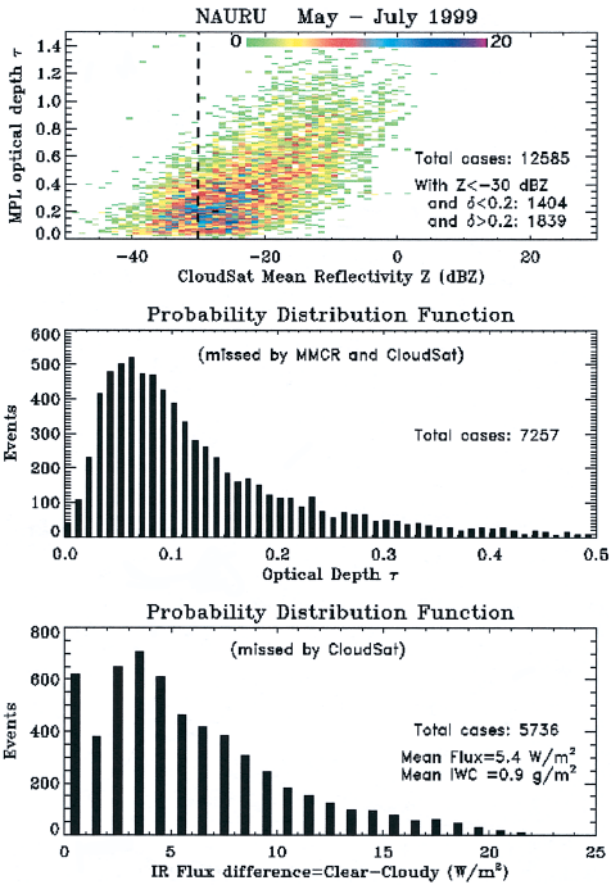

Fig. 11. (top) An example of the joint statistics obtained from combined lidar and radar measurements of tropical thin cirrus (adapted from Mitrescu and Stephens 2002) collected over a 3-month period as part of the ARM Nauru Tropical Western Pacific CART site. These statistics are in the form of the optical depth of tropical cirrus derived from a lidar transmission and the radar reflectivity averaged over the layer of cirrus. The data do not represent all cirrus observed during that time but only thin cirrus that do not fully attenuate the lidar. (middle) and (bottom) The fraction of these clouds missed by a radar with equivalent MDS and vertical resolution properties of CloudSat. This fraction is expressed in terms of (middle) optical depth and (bottom) TOA outgoing longwave flux.

range of optical depths between 0.1 and 0.4 although variability exists about this range (upper panel). At Nauru, there is a prevalence of thin cirrus that lies below the detection threshold of the CloudSat-like radar (37% of all thin cirrus cases) but these cirrus have minimal impact on the water budget of the upper troposphere (average paths less than 1 g m^{-2}) and on the TOA longwave flux (with estimated average OLR effects of 5 W m^{-2}).

Far less is known about the reflectivity of the different types of underlying surfaces encountered by an orbiting spaceborne 94-GHz radar. What limited information is available indicates that surface reflectivities typically vary as a function of surface type and condition as influenced by vegetation, soil moisture, and snow depth among other factors over land and surface wind speed over oceans (Ulaby and Dobson 1989). Characterization of the 94-GHz surface reflectivity is an area of emerging research to be promoted through the CloudSat Project.

CLOUDSAT PRODUCTS. Table 3 lists the principal level-1 and -2 products. The primary product is the level-1B calibrated, range-resolved radar reflectivities and the essential level-2 products are the cloud profile properties derived from these radar data. Two classes of level-2 products are distinguished. The first are the standard data products deemed necessary to meet the objectives for the mission. The second are the experimental products that provide supplementary information that enhances the science of the mission. Level-2 products also include a subset of MODIS and AMSR-E radiance data, as well as a number of selected (level 2) MODIS and CERES products specifically matched to the CloudSat radar ground track. The latter products will be used primarily for diagnostic and comparative studies.

Although details of the CloudSat products are subjects of ongoing research and future papers, a brief comment on three level-2 products is warranted. The cloud geometric profile (2B-GEOPROF) is derived from a version of the SEM algorithm of Clothiaux et al. (1995, 1999). This algorithm uses a carefully tuned noise threshold to identify weak cloud reflections from background instrument noise. The liquid and ice water content products (2B-LWC, 2B-IWC, respectively) derive from algorithms predicated on exploiting the different properties of active (radar) and passive (MODIS) observing systems. The benefits of combining such data has been demonstrated for more than 20 years using measurements from both aircraft and ground-based lidar, radar, and radiometer systems (e.g., Platt et al. 1998; Matrosov et al. 1992; Mace et al. 1998; Wang and Sassen 2001; and many others). Specific details on the theoretical basis for the water and ice algorithms together with an evaluation of their performance are described in Austin and Stephens (2001), Austin et al. (2002, manuscript submitted to *J. Geophys. Res.,* hereafter AUSTIN), and Benedetti et al. (2002, manuscript submitted to *J. Geophys. Res.*).

CHALLENGES AND OPPORTUNITIES. Data collected previously as well as up to and beyond the launch continue to guide the development of algorithms and a deeper understanding of the synergy of the A-Train multisensor data. Despite substantial progress, significant ambiguities exist in interpreting the observations and further understanding is required. Likewise, areas also emerge where exciting opportunities exist for developing new observational approaches and new scientific information.

Areas of note are as follows: The evaluation of the sensitivity of the CloudSat radar and how cloud detection may be augmented by the other sensors of the A-Train is crucial. Evaluation must include quantification of the effects of underdetection on both the water budget and radiative budget of clouds.

The transition from cloud to precipitation is a source of uncertainty that needs further study. Whereas the presence of drizzle in clouds as an initial stage in the development of precipitation benefits the problem of detection, particularly for boundary layer clouds, it also complicates the estimation of cloud liquid water (e.g., Fox and Illingworth 1997). Although it may be straightforward to identify drizzle from a reflectivity threshold perspective (e.g., Frisch et al. 1995) or from combinations of reflectivity and cloud optical depth (AUSTIN), retrieval of quantitative information about cloud LWC in the presence of drizzle have not been developed. CloudSat provides an opportunity to address this problem through a combination of radar data with A-Train satellite radiance data.

Mixed-phase clouds pose further difficulties. Supercooled liquid water obviously coexists with ice, and detection of these mixtures, not to mention quantifying the water contents of each phase, remains an important and particularly challenging problem, not only from the perspective of observations but also from the perspective of parameterization of these processes in global models (e.g., Rotstayn et al. 2000). Radar data, combined with other A-Train data such as the depolarization information from the lidar and polarimetric reflectances from PARASOL, provide an opportunity to focus some attention on both the observational challenges associated with mixed-phase clouds as well as on the parameterization of the mixed-phase processes in global models.

The categorization and quantification of precipitation also require further research. Solid and liquid precipitation are readily detected by the CloudSat radar. Simulations indicate that liquid precipitation exceeding about 10 mm h^{-1} at the surface will fully attenuate the spaceborne 94 GHz radar in the lowest 1 km (Table 2b). L'Ecuyer and Stephens (2002), using synthetic radar data simulated with the TRMM GPROF database as input (Olsen et al. 1996), demonstrated that 94-GHz radar data is capable of providing meaningful estimates of surface rain rate to about 3 mm h^{-1}. Retrievals under higher precipitation rates suffer from significant attenuation. Ambiguity arising from this attenuation can be addressed with the inclusion of path attenuation information that extends the validity of surface precipitation information to about 5–8 mm h^{-1}. Research on possible ways of dealing with attenuation and precipitation validation activities is planned as part of the efforts associated with AMSR-E validation.

TABLE 3. List of CloudSat level-1 and level-2 products. Standard products will be processed by the DPC and made available for distribution to the general scientific community. Experimental products will be produced and archived by individual scientists and the list of these products is expected to grow. Level-2 data, archived at the pixel level, are also to be averaged over space and time to produce a series of level-3 products (not listed in table). A discussion of the level-3 products, general sampling characteristics of the mission and related sampling errors will be described elsewhere, although general information about the types of sampling errors expected for the time–space mean CloudSat products can be found in GEWEX (1994).

Product ID	Description	Principal inputs	Characteristics and references
		Standard products	
1A-AUX	Auxiliary data for navigation altitude assignments, raw CPR data.	Digital elevation maps, spacecraft ephemeris.	
1B-CPR	Calibrated radar reflectivities.	Radar power, calibration factors.	500-m vertical resolution; day and night.
2B-GEOPROF	Cloud geometric profile—expressed in terms of occurrence and reflectivity (significant echoes), also includes (gas) attenuation correction.	1B-CPR, AN-MODMASK. A modified version of this product that includes CALIPSO lidar data is planned.	500-m vertical resolution (but the lidar-radar product will have higher vertical resolution); day and night.
2B-CLDCLASS	Eight classes of cloud type, including precipitation, identification, and likelihood of mixed phase conditions.	Radar and other data from the constellation.	Wang and Sassen (2001); day and night.
2B-TAU	Cloud optical depth by layer.	2B-GEOPROF and MODIS-AUX radiances.	$\tau > 0.1$, 20% accuracy (goal); daytime only.
2B-LWC	Cloud liquid water content.	2B-GEOPROF and 2B-TAU.	500 m and 50%; day and night, daytime uses 2B-TAU, nighttime product will be inferior to daytime.
2B-IWC	Cloud ice water content.	2B-GEOPROF and 2B-TAU, temperature	500 m +100% to –50%; day and night; daytime product uses 2B-TAU, nighttime product is inferior to daytime product.
2B-FLXHR	Atmospheric radiative fluxes and heating rates.	2B-GEOPROF, 2B-TAU, 2B-LWC/IWC.	Resolve longwave fluxes at TOA and surface to ~10 W m^{-2} and equivalently in cloud heating ~±1 K day^{-1} km^{-1}.
		Auxiliary data	
MODIS-AUX	MODIS radiances and cloud mask.	Radiances from 23 of the MODIS channels ±35 km about CloudSat ground track.	
AN-STATVAR	Subset along track of forecast model state variables.	The subsetting details are currently under study.	
AN-AMSR	AMSR-E radiances		
		Selected experimental products	
Precipitation	Quantitative precipitation.	2B-GEOPROF and AN-AMSR radiances.	
Cloud phase	Discrimination of ice and liquid.	2B-GEOPROF, CALIPSO lidar, MODIS radiances.	
Cloud microphysics	Droplet size profiles, number concentrations.	2B-GEOPROF, 2B-TAU, CALIPSO lidar, MODIS radiances.	

THE VALIDATION PLAN. The evaluation of both the standard and experimental products is an important focus of ongoing research activities that can be expected to continue prior to and after launch. The intent of these activities is the following:

1) To determine the calibration accuracy of the radar, thereby verifying the output of the level-1B radar algorithm that produces calibrated radar reflectivity profiles.
2) To determine the location accuracy of the radar footprint to enable the merging of CloudSat data with other datasets.
3) To evaluate the CloudSat radar sensitivity and to validate the cloud profile product, cloud detection statistics, and how cloud detection is augmented by the other sensors of the A-Train.
4) To quantify both random and bias errors estimated by the retrieval methods. The sources of these two errors types include *model errors* associated with the way observations are modeled in the retrieval approach, *measurement errors* related to instrument performance, calibration, noise, etc., and *database errors* due to uncertainties in a priori databases used to constrain nonunique solutions (e.g., ambiguities associated with attenuated radar reflectivities, etc.) or to assign certain model parameters.

A number of specific activities are planned to quantify these errors and characterize the CloudSat observing system. Many of these activities are being carried out prior to launch whereas other activities will be required throughout all phases of the mission.

Sensor calibration and footprint location. The calibration of the radar provides an overall uncertainty attached to the individual reflectivities. The CloudSat radar calibration plan includes a routine and detailed system calibration both prior to launch and in flight, vicarious calibration associated with surface returns from the ocean, and direct measurement comparisons with independently calibrated airborne radar that are volume matched to the spaceborne radar. The expected absolute calibration accuracy is 1.5–2 dBZ. Knowledge of the footprint location will be confirmed on orbit using the ocean–land variation of surface reflectivities as the radar field of view crosses coastlines. This approach is expected to provide an independent way of locating the radar footprint with an accuracy of approximately 250 m.

Detection. The tuning of the detection algorithm is being developed prior to launch using available data from aircraft flights as well as cloud radar data from ARM adapted to simulate level-1B data. The performance of the detection algorithm is to be monitored statistically via comparisons with long-term surface measurement and, when possible, aircraft measurements volume-matched to the spaceborne radar measurements.

Ground truth. The objective of ground truth measurements is to confirm the total retrieval error (bias plus random) from all sources. Ground truth requires comparison with independent data obtained from, for example, in situ cloud microphysics probes (e.g., Fig. 12a). Unfortunately, such comparisons do not generally offer an "absolute" truth given the differences in sampling volumes. Despite this difficulty, ground truth exercises are the only way to estimate the difficult-to-determine systematic retrieval errors. Postlaunch ground truth efforts applied to the actual CloudSat products are currently being planned.

Component error analyses. This activity attempts to quantify individual error components of the retrieval system, in particular focusing on model and database errors. For clouds and precipitation, these are the most significant sources of error. The analyses rely on a variety of data sources including currently archived cloud physics data obtained from past aircraft measurement programs worldwide (e.g., AUSTIN) as well as on the systematic measurement activities of ARM. An example of this type of analysis is the confirmation of the theoretical relation between measurements of (one way) cloud attenuation as a function of cloud liquid water content by Vali et al. (1998). The coefficients and attached errors of the simple linear relationship between radar attenuation and liquid water content are examples of specific model parameters used in cloud liquid water retrievals (e.g., Austin and Stephens 2001).

Consistency analyses: For this activity, the retrieved information is compared to other retrieved information involving different physical assumptions and thus different forward models. One example is provided in the form of a comparison of cloud-radar-based LWP information matched and compared to LWP inferred from MODIS optical properties, or independently from microwave radiometer data (Fig. 12b).

The specific strategy proposed includes the following:

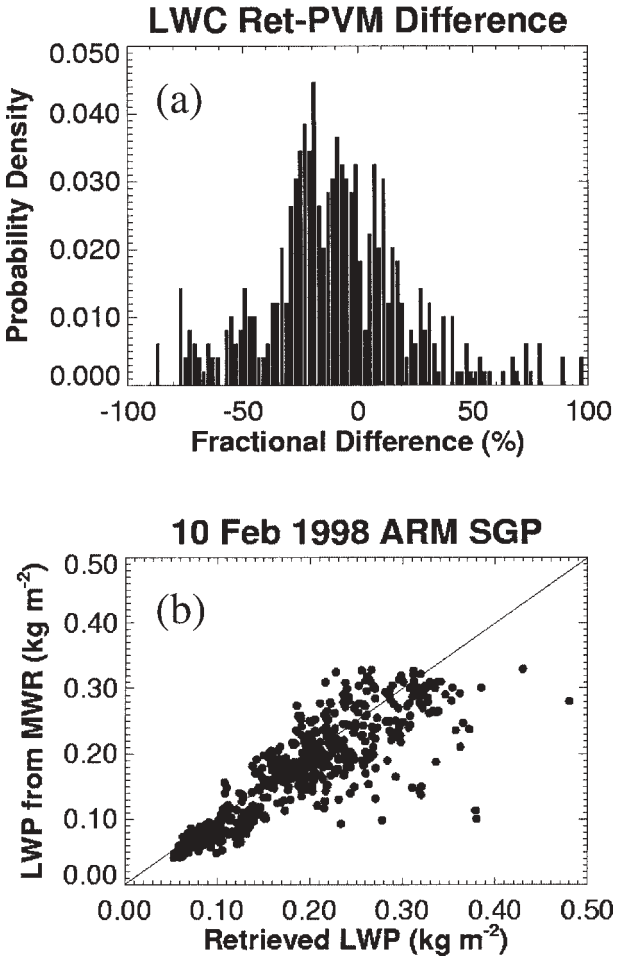

FIG. 12. (a) A form of ground truth of the CloudSat LWC algorithm. Shown is a probability density distribution of the differences of the liquid water content derived from two measurement sources. One source is from the CloudSat 2B-LWC algorithm applied to aircraft radar data and optical depth information obtained from reflected solar radiances measured by a spectrometer on the same aircraft. The second source is from an in situ Gerber (PVM) probe flown on a second aircraft profiling within the cloud. Only those in situ data deemed to lie within the radar volume are used. The rms of the differences is approximately 30% but this cannot be taken as a true measure of the total retrieval error for reasons mentioned in the text. The data are for a drizzle-free stratus cloud layer observed on 19 Jun 1999 off the west coast of California near Monterey. (b) The LWP derived using the CloudSat 2B-LWC algorithm applied to ARM-CART cloud radar data and coincident optical depth from Min and Harrison (1996) analyses of cloud optical depth compared to LWP obtained from the ARM microwave radiometer for nondrizzle clouds (AUSTIN).

1) Application of algorithms to synthetic data for which the actual cloud information is known. An example of this approach is described in the study of Sassen et al. (2002) who employ an explicit cirrus microphysical model to simulate time-evolving radar reflectivities, lidar backscatter, and optical depths.
2) Comparison of products derived from different algorithms based on different kinds of forward model assumptions and data inputs. For example, the ice water contents derived from simpler CloudSat-like algorithms can be compared to equivalent information derived from algorithms that use either additional radar data such as reflectivity at a different frequency (Sekelsky et al. 1999) or reflectivity data plus Doppler moment data (Clothiaux et al. 2000) or entirely different sensor data as in the example of microwave radiometer cloud liquid water path data (e.g., AUSTIN).
3) Application of the algorithms to surface-based radar data that are subsequently evaluated using information matched to the radar volumes obtained from airborne platforms with necessary cloud microphysical sensors.
4) Similar to 2) but using aircraft radar and radiometer data matched to measurements from in situ aircraft sensors of relevant cloud parameters in a manner similar to that reported in the study of AUSTIN.
5) Similar to 4) matching aircraft in situ data with satellite data after launch.

The CloudSat validation plan benefits from the systematic measurement programs of ARM that focus on use of surface remote sensors as well as systematic measurements planned for selected sites within Europe and Japan. The validation plan also benefits from regular aircraft radar measurement activities within the United States, Japan, and Europe; the measurement capabilities at a number of universities (such as Sassen et al. 2001); and cloud field program activities representing targets of opportunity planned in the coming years. CloudSat also has begun to link to the validation activities of CALIPSO as well as to the validation activities planned for *Aqua*.

SUMMARY. CloudSat is designed to measure the vertical structure of clouds and precipitation from space and does so through the first spaceborne flight of a 94-GHz cloud profiling radar. Not only will this mission stimulate important new research on clouds and precipitation, but it will also provide an important demonstration of 94-GHz radar technology in a space-borne application.

CloudSat employs a measurement and algorithm approach that combines radar information with ra-

diance data obtained from other sensors of the constellation. Information derived from this combination, summarized in Table 3, includes detailed vertical profile information about the water and ice contents of clouds, the occurrence of precipitation as well as some quantitative information about precipitation. CloudSat will provide a large and unique ensemble of these properties that will uncover new knowledge about clouds and precipitation and the connection of clouds to the large-scale motions of the atmosphere, offer probing tests of global climate and weather forecast models as well as cloud resolving models and related parameterizations. As such, CloudSat will provide new ways of examining relationships between clouds and other properties of the atmosphere that are important for understanding the earth's hydrological cycle and how cloud feedbacks are established within the climate system.

At present the science team is confined to a limited number of researchers who are responsible for developing the algorithms of the standard products and for developing the steps to validate these products. The team will expand near the time of launch. At that time, NASA will support a larger team and the research of the wider community encouraging use of CloudSat data in the study of clouds and climate.

ACKNOWLEDGMENTS. The research described in this paper was carried out at a number of institutions, including the Jet Propulsion Laboratory, California Institute of Technology, under a contract with the National Aeronautics and Space Administration. This research was also supported by NASA Contract NAS 5-99237, Jet Propulsion Laboratory, California Institute of Technology Contracts 1212032 and 961158 at Colorado State University.

APPENDIX A: LIST OF ACRONYMS

AFSCN	Air Force Satellite Control Network
AMIP-II	Atmospheric Model Intercomparison Project II
AMSR-E	Advanced Microwave Scanning Radiometer for EOS
ARM	Atmospheric Radiation Measurement Program
BATC	Ball Aerospace (Boulder, CO)
CALIPSO	Cloud-Aerosol Lidar and Infrared Pathfinder Satellite Observations
CART	Cloud and Radiation Testbed
CDF	Cumulative distribution functions
CERES	Clouds and the Earth's Radiant Energy System
CIRA	Cooperative Institute for Research in the Atmosphere
CNES	Centre National d'Études Spatiales
CORE	CloudSat Operational and Research Environment
CSU	Colorado State University
DAAC	Distributed Active Archive Center
DOE	Department of Energy
DPC	Data Processing Center
DPEAS	Data Processing and Error Analysis System
EIK	Extended interaction klystron
EOS	Earth Observing System
ESSP	Earth System Science Pathfinder
FOV	Field of view
GEWEX	Global Energy and Water Experiment
HDF-EOS	Hierarchical Data Format-Earth Observing System
HPA	High power amplifier
IPCC	Intergovernmental Panel on Climate Change
ISCCP	International Satellite Cloud Climatology Project
JPL	Jet Propulsion Laboratory
KAFB	Kirtland Air Force Base (Albuquerque, NM)
LWP	Liquid water path
MDS	Minimum detectable signal
MODIS	Moderate-Resolution Imaging Spectroradiometer
NWP	Numerical weather prediction
OAS	Onizuka Air Force Station (Sunnyvale, CA)
PARASOL	Polarisation et Anisotropie des Réflectances au sommet de l'Atmospherè, couplées avec in Satellite d'Observation emportant un Lidar
PR	Precipitation radar
QOTL	Quasi-optical transmission line
RFES	Radio frequency electronics subsystem
RSC	RTD&E (Research, Testing, Development, and Engineering) Support Center
SAFB	Schriever Air Force Base (Colorado Springs, CO)
SEM	Significant echo mask
SGLS	Space Ground Link Subsystem
TOA	Top of the atmosphere
TRMM	Tropical Rainfall Measuring Mission
VAFB	Vandenberg Air Force Base
WRS	World Reference System

APPENDIX B: OVERVIEW OF THE CLOUDSAT MEASUREMENT REQUIREMENTS. One of the key objectives of the mission is to be able to provide information sufficient for determining the

contribution of clouds to the radiative heating of the atmosphere. This contribution, and the radiative fluxes that determine it, are provided by the 2B-FLXHR product (Table 3).

Accuracy requirements placed on the level-2 products were established by tracing these requirements back to a requirement established for the radiative heating and related radiative fluxes. Although measurement requirements for TOA fluxes are documented (e.g., Wielicki et al. 1996), it is neither a straightforward nor obvious task to relate these TOA flux requirements to heating rates. The approach developed to establish the heating rate requirement connects variations in cloud radiative heating to changes in observable quantities; atmospheric temperature and precipitation are chosen since measurement requirements exist for these parameters. The relation between cloud radiative heating rates, temperature, and precipitation was established using two general circulation models (Schneider and Stephens 1996). This further provided a way of connecting TOA fluxes to cloud radiative heating, thereby providing a connection to the documented TOA and surface flux requirements of CERES. These flux requirements represent a more tangible way of establishing accuracy requirements on optical depth, liquid and ice water contents, and minimum radar detection thresholds (Miller and Stephens 2001).

The results of the above mentioned studies may be summarized as follows:

1) GCM sensitivity studies suggest that changing in-cloud radiative heating by an amount of 1 K day^{-1} over a 1-km layer leads to predicted changes in the precipitation rate in the Tropics of about 10% and changes to atmospheric temperature globally of 1–2 K. The latter are consistent with present capabilities to measure atmospheric temperature, and the precipitation changes are slightly below with the measurement capabilities presently understood for TRMM. The changes to temperature and precipitation are also consistent with the along-track estimation of instantaneous longwave exitant fluxes within 5–10 W m^{-2} at the top and bottom of the atmosphere.
2) TOA longwave fluxes, derived by comparing simulations that contain ±20% differences in cloud optical depth and liquid water content, compared to control simulations are within ±5 W m^{-2} of the control simulations (Miller and Stephens 2001).
3) Based on realistic assumptions for the particle sizes of ice and water clouds, a radar with a minimum sensitivity of –28 dB*Z* will miss some optically thin high clouds and a higher fraction of low clouds (note also Figs. 10 and 11). Although we do not know these statistics on the global scale, we estimated that a radar-only system operating with a minimum sensitivity of –28 dB*Z* will detect approximately 90%–95% of all ice mass and perhaps as much as 80% of the water mass. However, when combined with other radiance observations (such as available from MODIS), many of the undetected low water clouds will also be counted and further improvement for ice content is expected with the addition of CALIPSO lidar observations. Overall, our best estimate is that the clouds missed by CloudSat will impact the in-cloud radiative heating by less than 1K day^{-1} km^{-1}.
4) The clouds missed by the radar lead to an underestimate of the instantaneous TOA and surface longwave fluxes, largely by missing some fraction of low clouds. When detection of low thin clouds by the radar is augmented by radiance data from *Aqua,* it is expected that these longwave flux errors will be reduced to approximately 5 W m^{-2}.
5) The corresponding visible optical depths of clouds undetected by a radar-only observing system operating with a –28 dB*Z* MDS varies with particle size. Assuming particle sizes typical of those observed, the threshold radar detection is about $\tau \approx 1$–5 for low-level water clouds and $\tau \approx 0.1$–0.4 for ice clouds. These values vary according to the cloud microphysics.

REFERENCES

Austin, R. T., and G. L. Stephens, 2001: Retrieval of stratus cloud microphysical parameters using millimeter-wave radar and visible optical depth in preparation for CloudSat. 1. Algorithm formulation. *J. Geophys. Res.,* **106,** 28 233–28 242.

——, ——, S. D. Miller, S. M. Sekelsky, F. Li, and Q. Min, 2002: Retrieval of stratus cloud microphysical parameters using millimeter-wave radar and visible optical depth in preparation for CloudSat. 2. Algorithm evaluation. *J. Geophys. Res.,* submitted.

Battan, L. J., 1973: *Radar Observations of the Atmosphere.* University of Chicago Press, 324 pp.

Benedetti, A., G. L. Stephens, and J. Haynes, 2002: Ice cloud microphysical retrievals from millimeter radar and visible optical depth using an estimation theory approach. *J. Geophys. Res.,* submitted.

Cess, R. D., and Coauthors, 1989: Interpretation of cloud-climate feedback is produced by 14 atmospheric general circulation models. *Science,* **245,** 513–516.

Clothiaux, E. E., M. A. Miller, B. A. Albrecht, T. P. Ackerman, J. Verlinde, D. M. Babb, R. M. Peters, and W. J. Syrett, 1995: An evaluation of a 94 GHz radar for remote sensing of cloud properties. *J. Atmos. Oceanic Technol.,* **12,** 201–229.

——, and Coauthors, 1999: The Atmospheric Radiation Measurement program cloud radars: Operational modes. *J. Atmos. Oceanic Technol.,* **16,** 819–827.

——, T. P. Ackerman, G. G. Mace, K. P. Moran, R. T. Marchand, M. A. Miller, and B. E. Martner, 2000: Objective determination of cloud heights and radar reflectivities using a combination of active remote sensors at the ARM CART sites. *J. Appl. Meteor.,* **39,** 645–665.

Deschamps, P. Y., F. M. Breon, M. Leroy, A. Podaire, A. Bricaud, J. C. Buriez, and G. Seze, 1994: The POLDER mission: Instrument characteristics and scientific objectives. *IEEE Trans. Geosci. Remote Sensing.,* **32,** 598–615.

Fowler, L. D., and D. A. Randall, 1994: A global radiative–convective feedback. *Geophys. Res. Lett.,* **21,** 2035–2038.

——, ——, and S. A. Rutledge, 1996: Liquid and ice cloud microphysics in the CSU general circulation model. Part I: Model description and simulated microphysical processes. *J. Climate,* **9,** 489–529.

Fox, N. I., and A. J. Illingworth, 1997: The retrieval of stratocumulus cloud properties by ground-based cloud radar. *J. Appl. Meteor.,* **36,** 485–492.

Frisch, A. S., C. W. Fairall, and J. B. Snider, 1995: Measurements of stratus cloud and drizzle parameters in ASTEX with Ka-band Doppler radar and microwave radiometer. *J. Atmos. Sci.,* **52,** 2788–2799.

GEWEX, 1994: Utility and feasibility of cloud profiling radar. International GEWEX Project Office, World Climate Research Programme, Publ. No. 10, 92 pp.

Gleckler, P. J., and Coauthors, 1995: Cloud-radiative effects on implied oceanic energy transports as simulated by atmospheric general circulation models. *Geophys. Res. Lett.,* **22,** 791–794.

Grabowski, W.W., J.-I. Yano, and M. W. Moncrieff, 2000: Cloud resolving modeling of tropical circulations driven by large-scale SST gradients. *J Atmos. Sci.,* **57,** 2022–2039.

Harrison, E. F., P. Minnis, B. R. Barkstrom, and G. G. Gibson, 1993: Radiation budget at the top of the atmosphere. *Atlas of Satellite Observations Related to Global Change,* R. J. Gurney, J. L. Foster, and C. L. Parkinson, Eds., Cambridge University Press, 19–38.

Jakob, C., and S. A. Klein, 1999: The role of vertically varying cloud fraction in the parameterization of microphysical processes in the ECMWF model. *Quart. J. Roy. Meteor. Soc.,* **125,** 941–965.

Jones, A. S., and T. H. Vonder Haar, 2001: Overview of an HDF-EOS-based parallel data computing environment for multisensor satellite data merger and scientific analysis. Preprints, *17th Conf. on Interactive Information and Processing Systems (IIPS) for Meteorology, Oceanography, and Hydrology,* Albuquerque, NM, Amer. Meteor. Soc., 329–332.

Kandel, R., and Coauthors, 1998: The ScaRaB Earth radiation budget datasets. *Bull. Amer. Meteor. Soc.,* **79,** 765–783.

L'Ecuyer, T. S., and G. L. Stephens, 2002: An estimation-based precipitation retrieval algorithm for attenuating radars. *J. Appl. Meteor.,* **41,** 272–285.

Liang, X.-Z., and W.-C. Wang, 1997: Cloud overlap effects on GCM climate simulations. *J. Geophys. Res.,* **102,** 11 039–11 047.

Ma, C. C., C. R. Mechoso, A. Arakawa, and J. Farrara, 1994: Sensitivity of a coupled ocean–atmosphere model to physical parameterizations. *J. Climate,* **7,** 1883–1896.

Mace, G. G., C. Jakob, and K. P. Moran, 1998: Validation of hydrometeor occurrence predicted by the ECMWF model using millimeter wave radar data. *Geophys. Res. Lett.,* **25,** 1645–1648.

Matrosov, S. Y., T. Uttal, J. B. Snider, and R. A. Kropfli, 1992: Estimation of ice cloud parameters from ground-based infrared radiometer and radar measurements. *J. Geophys. Res.,* **97,** 20 675–20 683.

Menzel, P. W., 2001: Cloud tracking with satellite imagery: From the pioneering work of Ted Fujita to the present. *Bull. Amer. Meteor. Soc.,* **82,** 33–47.

Miller, S. D., and G. L. Stephens, 2001: CloudSat instrument requirements as determined from ECMWF forecasts of global cloudiness. *J. Geophys. Res.,* **106,** 17 713–17 733.

Min, Q., and L. C. Harrison, 1996: Cloud properties derived from surface MFRSR measurements and comparisons with GOES results at the ARM SGP site. *Geophys. Res. Lett.* **23,** 1641–1644.

Mitrescu, C., and G. L. Stephens, 2002: A new method for determining cloud transmittance and optical depth using the ARM Micro-Pulsed Lidar. *J. Atmos. Oceanic Technol.,* **19,** 1073–1081.

Moran, K. P., B. E. Martner, M. J. Post, R. A. Kropfli, D. C. Welsh, and K. Widener, 1998: An unattenuated cloud-profiling radar for use in climate research. *Bull. Amer. Meteor. Soc.,* **79,** 443–455.

Olson, W. S., C. D. Kummerow, G. M. Heymsfield, and L. Giglio, 1996: A method for combined passive-active microwave retrievals of cloud and precipitation profiles. *J. Appl. Meteor.,* **35,** 1763–1789.

Parsons, D. B., K. Yoneyama, and J.-L. Redelsperger, 2000: Evolution of the tropical western Pacific atmosphere–

ocean system following the arrival of a dry intrusion. *Quart. J. Roy. Meteor. Soc.,* **126,** 517–548.

Platt, C. M. R., S. A. Young, P. J. Manson, G. R. Patterson, S. C. Marsden, R. T. Austin, and J. Churnside, 1998: The optical properties of equatorial cirrus from observations in the ARM pilot radiation observation experiment. *J. Atmos. Sci.,* **55,** 1977–1996.

Poore, K. D., J. Wang, and W. B. Rossow, 1995: Cloud layer thicknesses from a combination of surface and upper-air observations. *J. Climate,* **8,** 550–568.

Randall, D. A., Harshvardhan, D. A. Dazlich, and T. G. Corsetti, 1989: Interactions among radiation, convection and large-scale dynamics in a general circulation models. *J. Atmos. Sci.,* **46,** 1943–1970.

Rogers, R. R., 1979: *A Short Course in Cloud Physics.* 2d ed. Pergamon Press, 235 pp.

Rossow, W. B., and B. Cairns, 1995: Monitoring changes of clouds. *Climatic Change,* **31,** 305–347.

——, and R. A. Schiffer, 1999: Advances in understanding clouds from ISCCP. *Bull. Amer. Meteor. Soc.,* **80,** 2261–2287.

Rotstayn, L. D., B. F. Ryan, and J. J. Katzfey, 2000: A scheme for calculation of the liquid fraction in mixed-phase stratiform clouds in large-scale models. *Mon. Wea. Rev.,* **128,** 1070–1088.

Sassen, K., J. M. Comstock, Z. Wang, and G. G. Mace, 2001: Cloud and aerosol research capabilities at FARS: The Facility for Atmospheric Remote Sensing. *Bull. Amer. Meteor. Soc.,* **82,** 1119–1138.

Schneider, T. L., and G. L. Stephens, 1996: Climatically relevant clouds as seen by a spaceborne radar, lidar, and submillimeter-wave radiometer. *Proceedings of the International Radiation Symposium: Current Problems in Atmospheric Radiation,* W. L. Smith and K. Stamnes, Eds., A. Deepak, 651–654.

Sekelsky, S. M., W. L. Ecklund, J. M. Firda, K. S. Gage, and R. E. McIntosh, 1999: Particle size estimation in ice-phase clouds using multifrequency radar reflectivity measurements at 95, 33, and 2.8 GHz. *J. Appl. Meteor.,* **38,** 5–28.

Senior, C. A., and J. F. B. Mitchell, 1993: Carbon dioxide and climate: The impact of cloud parameterization. *J. Climate,* **6,** 393–418.

Simpson, J., C. Kummerow, W. K. Tao, and R. F. Adler, 1996: On the Tropical Rainfall Measuring Mission (TRMM). *Meteor. Atmos. Phys.,* **60,** 19–36.

Slingo, A., and J. M. Slingo, 1988: Response of a general circulation model to cloud long-wave radiative forcing. Part I: Introduction and initial experiments. *Quart. J. Roy. Meteor. Soc.,* **114,** 1027–1062.

Stephens, G. L., 1978: Radiation profiles in extended water clouds: Parameterization schemes. *J. Atmos. Sci.,* **35,** 2123–2132.

——, 1999: Radiative effects of clouds and water vapor. *Global Energy and Water Cycles,* K. A. Browing, and R. J. Gurney, Eds., Cambridge University Press., 71–90.

——, 2001: Cirrus, climate and global change. *Cirrus,* D. Lynch et al., Eds., Oxford University Press, 433–448.

——, C. Jakob, and M. Miller, 1998: Atmospheric ice—A major gap in understanding the effects of clouds on climate. *GEWEX News,* **8,** 1–8.

Stokes, G. M., and S. E. Schwartz, 1994: The Atmospheric Radiation Measurement (ARM) Program: Programmatic background and design of the cloud and radiation test bed. *Bull. Amer. Meteor. Soc.,* **75,** 1201–1221.

Sundquist, H., 1978: Parameterization scheme for nonconvective condensation, including prediction of cloud water content. *Quart. J. Roy. Meteor. Soc.,* **104,** 677–690.

Tiedtke, M., 1993: Representation of clouds in large-scale models. *Mon. Wea. Rev.,* **121,** 3040–3061.

Ulaby, F. T., and M. C. Dobson, 1989: *Handbook of Radar Scattering Statistics for Terrain.* Artech House, 357 pp.

Vali, G., R. D. Kelly, J. French, S. Haimov, D. Leon, R. E. McIntosh, and A. Pazmany, 1998: Finescale structure and microphysics of coastal stratus. *J. Atmos. Sci.,* **55,** 3540–3564.

Wang, J.-H., W. B. Rossow, and Y.-C. Zhang, 2000: Cloud vertical structure and its variations from a 20-year global rawinsonde dataset. *J. Climate,* **13,** 3041–3056.

Wang, Z., and K. Sassen, 2001: Cloud type and macrophysical property retrieval using multiple remote sensors. *J. Appl. Meteor.,* **40,** 1665–1682.

Webster, P. J., and G. L. Stephens, 1983: Cloud-radiation interaction and the climate problem. *The Global Climate,* J. T. Houghton, Ed., Cambridge University Press, 63–78.

Wielicki, B. A., R. D. Cess, M. D. King, D. A. Randall, and E. F. Harrison, 1995: Mission to planet Earth: Role of clouds and radiation in climate. *Bull. Amer. Meteor. Soc.,* **76,** 2125–2153.

——, B. R. Barkstrom, E. F. Harrison, R. B. Lee, G. L. Smith, and J. E. Cooper, 1996: Clouds and the Earth's Radiant Energy System (CERES): An Earth Observing System experiment. *Bull. Amer. Meteor. Soc.,* **77,** 853–868.